


Review

State of the Art of CFD-DEM Coupled Modeling and Its Application in Turbulent Flow-Induced Soil Erosion

Jun Xu ^{1,*}, Fei Wang ^{2,*} and Ruth Abegaz ¹ 

¹ Department of Mechanical, Environmental, and Civil Engineering, Mayfield College of Engineering, Tarleton State University, Stephenville, TX 76401, USA; rabegaz@tarleton.edu

² Richard A. Rula School of Civil and Environmental Engineering, Mississippi State University, Mississippi State, MS 39762, USA

* Correspondence: junxu@tarleton.edu (J.X.); feiwang@cee.msstate.edu (F.W.)

Abstract: Fluid–soil interaction plays a pivotal role in various geotechnical engineering applications, as it significantly influences processes such as erosion, sediment transport, and soil stability. Modeling fluid–soil particle interactions in these contexts presents substantial challenges due to the inherent complexity of the interactions occurring across multiple characteristic scales. The primary challenge lies in the vast disparities in magnitude between these scales, which demand sophisticated modeling techniques to accurately capture the intricate dynamics involved. Coupled fluid–soil particle models have emerged as essential tools for understanding the mechanisms underlying fluid–soil interactions. Among these, the CFD-DEM (computational fluid dynamics–discrete element method) approach has gained significant attention. This method provides an effective compromise between high-resolution sub-particle fluid modeling and coarser mesh-based techniques for fluids and particles. By doing so, CFD-DEM facilitates large-scale simulations while maintaining computational efficiency, making it a promising solution for studying fluid–soil interactions in complex geotechnical scenarios. This review highlights the application of CFD-DEM models in geotechnical engineering, with a specific focus on soil erosion processes and the critical role of turbulent flow. It explores various fluid–soil particle interaction computational mechanisms and their implications for erosion dynamics, emphasizing several key aspects, including the following: laminar vs. turbulent flow models: understanding the distinctions between flow regimes is critical for accurately predicting fluid-induced soil particle movement. Shear stress effects: the influence of flow-induced shear stress on the detachment of soil particles is analyzed, particularly in erosion-prone environments. Sediment transport mechanisms: factors such as particle size, density, and water velocity are examined for their roles in governing sediment transport. Knowledge gaps and future directions: these involve identifying unresolved issues in current fluid–soil interaction models, with an emphasis on improving the accuracy and scalability of CFD-DEM simulations. By delving into these aspects, the review aims to advance the understanding of fluid–soil interactions and provide insights into optimizing modeling techniques for geotechnical engineering applications. It also outlines future research directions to bridge existing knowledge gaps, emphasizing the importance of integrating advanced turbulence modeling and computational strategies to enhance the predictive capabilities of fluid–soil interaction frameworks.



Academic Editor: Mohamed Shahnin

Received: 19 November 2024

Revised: 16 December 2024

Accepted: 8 January 2025

Published: 10 January 2025

Citation: Xu, J.; Wang, F.; Abegaz, R. State of the Art of CFD-DEM Coupled Modeling and Its Application in Turbulent Flow-Induced Soil Erosion. *Geosciences* **2025**, *15*, 21. <https://doi.org/10.3390/geosciences15010021>

Copyright: © 2025 by the authors. Licensee MDPI, Basel, Switzerland.

This article is an open access article distributed under the terms and conditions of the Creative Commons Attribution (CC BY) license (<https://creativecommons.org/licenses/by/4.0/>).

Keywords: soil erosion; computational fluid dynamics; discrete element method; CFD-DEM coupling; geotechnical engineering

1. Introduction

Soil erosion is a natural process where soil particles are removed and transported by external agents such as wind, water, and gravity [1,2]. While erosion is an essential component of the Earth's geologic cycle, human activities like agriculture, deforestation, and urbanization have accelerated its pace, leading to significant environmental, economic, and societal impacts [3,4]. Soil erosion can result in the loss of fertile topsoil, reduced agricultural productivity, sedimentation in water bodies, and the degradation of natural ecosystems [5,6]. Among the various forms of erosion, water-induced soil erosion is particularly critical, as it contributes to a substantial portion of land degradation globally [7].

Water-induced erosion is driven primarily by rainfall, surface runoff, and streamflow, which trigger different erosion mechanisms [8]. These include splash erosion [9], where raindrop impacts dislodge soil particles; sheet erosion [10], where a thin layer of soil is removed by surface water flow; rill erosion [10], which forms small channels as water concentrates and flows more forcefully; and gully erosion [11], which involves larger, more destructive channels. Understanding the fluid dynamics behind these processes is vital for predicting and mitigating soil erosion.

This review explores the fluid dynamics of soil erosion, with a specific focus on the role of turbulent flow in the erosion process. The distinction between laminar and turbulent flow is crucial in understanding how different flow regimes affect soil particle detachment and transport. Laminar flow, characterized by smooth and orderly fluid motion, exerts lower forces on soil particles, whereas turbulent flow, with its chaotic and fluctuating motion, creates higher shear stress, significantly increasing the potential for erosion [12–14].

This review will examine the key concepts of fluid dynamics in soil erosion, emphasizing the interplay between flow conditions, shear stress, and sediment transport. By understanding these processes, we can develop better strategies for erosion control and landscape management.

2. Fluid–Soil Interaction

Fluid–soil interaction (FSI) plays a key role in understanding the mechanics of granular soils [15]. FSI governs complex processes such as sediment transport [16,17], internal erosion [18], sand liquefaction [19], and debris flow [20]. These processes are not only critical to geological formations but also have significant implications in geotechnical engineering, where the stability of soil structures, foundation systems, and embankments depends on the interaction between fluid flow and soil particles. Understanding these interactions at the micro and macro scales is essential for mitigating risks such as erosion, landslides, and other geotechnical hazards.

One fundamental aspect of FSI is the interaction between fluid and soil particles, especially in saturated soils. In such systems, fluid flow through the pore spaces between particles affects the overall mechanical behavior of the soil. This interaction can disturb pore water pressure, leading to phenomena such as seepage, consolidation, or liquefaction. However, due to the complexity of these interactions, accurately monitoring and quantifying them in laboratory settings remains challenging. Thus, advanced numerical methods, such as the discrete element method (DEM) and computational fluid dynamics (CFD), have been developed to simulate fluid–soil interactions at the particle scale, offering a more detailed understanding of these mechanisms [21].

2.1. Numerical Methods in Fluid–Soil Interaction

Numerical simulation has become an invaluable tool for studying FSI, particularly where laboratory experimentation has limits as to what level of details can be revealed. Traditional methods for modeling fluid flow, such as the Navier–Stokes equations, are solved through various computational fluid dynamics (CFD) approaches.

Turbulent computational fluid dynamics (CFD) methods are techniques used to model and simulate the chaotic irregular behavior of turbulence in fluid flows. Since turbulence involves a wide range of scales, from large eddies to very small fluctuations, these methods aim to capture the key aspects of turbulent behavior while balancing computational cost and accuracy. Below is a summary of the main turbulent CFD methods in Table 1.

Table 1. Turbulence computational models.

Turbulence Models	Overview	Pros	Cons
Direct Numerical Simulation (DNS) [22–25]	DNS solves the full Navier–Stokes equations without any turbulence modeling, capturing all scales of turbulence down to the smallest scales or Kolmogorov scales.	Highly accurate and detailed representation of turbulence.	Extremely computationally expensive, making it feasible only for low-Reynolds-number flows and simple geometries.
Large Eddy Simulation (LES) [26–29]	LES directly resolves the larger turbulent eddies while modeling the smaller, more universal scales. This is achieved using a filter that separates large and small eddies, with only the small scales being modeled.	More computationally efficient than DNS and captures essential turbulent structures. Suitable for complex flows and geometries.	Still computationally demanding, especially near walls where turbulence scales are small, so LES is generally used for high-Reynolds-number flows with coarse grid near-wall models or in regions where finer detail is needed.
Reynolds-Averaged Navier–Stokes (RANS) [30–34]	RANS methods solve for time-averaged flow properties and use turbulence models to account for the effects of turbulence. RANS simplifies the Navier–Stokes equations by decomposing flow quantities into mean and fluctuating components. Common RANS models include the following: k- ϵ model: widely used for general-purpose turbulence modeling, especially for free-shear flows (e.g., jet flows). k- ω model: performs better in adverse pressure gradients and boundary layers, making it more suitable for wall-bounded flows. Reynolds stress model (RSM): accounts for anisotropy in turbulence by directly modeling the Reynolds stresses, leading to greater accuracy but also higher computational costs.	Much more computationally efficient than DNS and LES, making it the most common approach for industrial applications.	Less accurate for complex turbulent flows, since the averaged models can oversimplify turbulence structures.
Hybrid RANS-LES Models [35–38]	These models combine the RANS and LES approaches, often using RANS in near-wall regions and LES in the core flow regions where large eddies are dominant. Detached eddy simulation (DES): switches from RANS to LES based on grid size and turbulence scale. Scale-adaptive simulation (SAS): adjusts the turbulence model dynamically based on the local flow conditions, useful in flows with large separation zones. Delayed detached eddy simulation (DDES): a modification of DES that delays the transition to LES, minimizing grid-size dependency issues.	Balances computational cost and accuracy, providing a feasible way to capture large-scale turbulence in regions that require it while maintaining efficiency near walls.	Hybrid methods can be complex to implement, as they require a seamless transition between RANS and LES zones.

Table 1. Cont.

Turbulence Models	Overview	Pros	Cons
Wall-Modeled LES (WMLES) [39–41]	This is a variant of LES that applies a wall model near solid boundaries, allowing for coarser grids near walls while still resolving large eddies away from the wall.	Reduces the computational cost of LES by simplifying the near-wall region.	Wall models can introduce inaccuracies, especially if the model is not well-tuned to the specific flow.
Partially Averaged Navier–Stokes (PANS) [42–45]	PANS is a variable-resolution method that blends between DNS, LES, and RANS depending on the level of filtering applied. It allows users to set a level of detail based on available computational resources and desired accuracy.	Offers flexibility to adjust turbulence modeling fidelity, making it adaptable for various flow regimes.	Complexity in adjusting the filtering level for consistent and reliable results across different flow regions.

These methods allow CFD analysts to choose the level of turbulence modeling needed for a particular application, balancing the trade-off between computational cost and the level of detail in turbulent flow structures.

These CFD methods are typically coupled with particle-scale models. Several particle-based methods have been used for the modeling of the mechanical behavior of granular soils and the soil–fluid interactions, such as smooth particle hydrodynamics (SPH) [46–49], the discrete element method (DEM) [15,46,50–80], and the material point method (MPM) [81–87], all demonstrate highly realistic responses in modeling large deformation problems. Each of these numerical methods has been instrumental in advancing simulations of complex materials and interactions under significant deformation, where conventional methods often fall short. SPH is particularly effective for fluid simulations, while DEM is well-suited for capturing the mechanics of granular soils and for describing particle flows under Newton’s laws of motion, and MPM provides robust capabilities for solid mechanics. SPH and MPM are continuum models and yield limited information concerning the particle-scale soil behavior. Due to these limitations, we will focus on the DEM, especially computational fluid dynamics–discrete element method (CFD-DEM) coupling methods, in this review.

2.2. CFD-DEM Coupled Models

In DEM models, each real particle in granular soils is modeled individually and the particle contact physics is resolved. Therefore, the DEM has advantages in modeling the particle-scale movements and interactions in granular soils (Figure 1). When combined with CFD, the CFD-DEM coupling models enable the simultaneous simulation of fluid flow and particle collisions, capturing the fluid–solid interactions that are critical in geotechnical applications. Based on mesh resolution in the fluid phase, the CFD-DEM model can be categorized into the unresolved (Figure 2) and fully resolved models (Figure 3) [88,89]. A compromise between resolved and unresolved CFD-DEM is called semi-resolved CFD-DEM (Figure 4), which uses various kernel functions to improve the void fraction models and reduce computational errors [83,89–93]. The semi-resolved CFD-DEM approach, while exhibiting limitations in accuracy due to its combination of theoretical and empirical models, is nonetheless well-suited to industrial applications. This balance between theory and empirical adjustments allows for a practical level of accuracy that meets the needs of many complex simulations. Additionally, the semi-resolved CFD-DEM model offers valuable strengths across several areas, namely that it achieves a favorable balance of accuracy and efficiency, making it computationally feasible for large-scale applications. Its adaptability to various particulate flow scenarios, along with its ability to describe complex fluid–particle interactions in granular materials, further enhances its utility in a wide range

of engineering and industrial contexts. The ratio of grid to particle size for unresolved, resolved, and semi-resolved models is shown in Figure 1 for Figures 2–4, respectively.

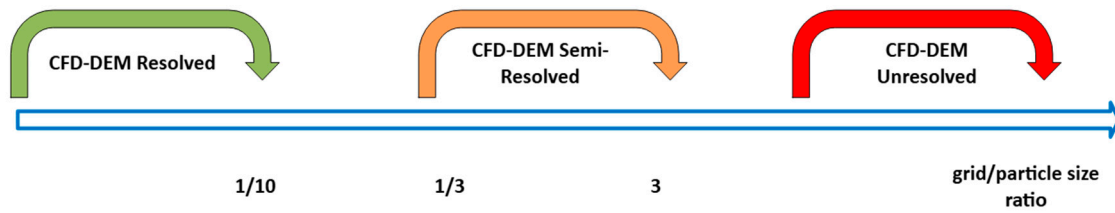


Figure 1. Regions of the mesh–particle size ratio for resolved, semi-resolved, and unresolved CFD-DEM adopted from [89,91].

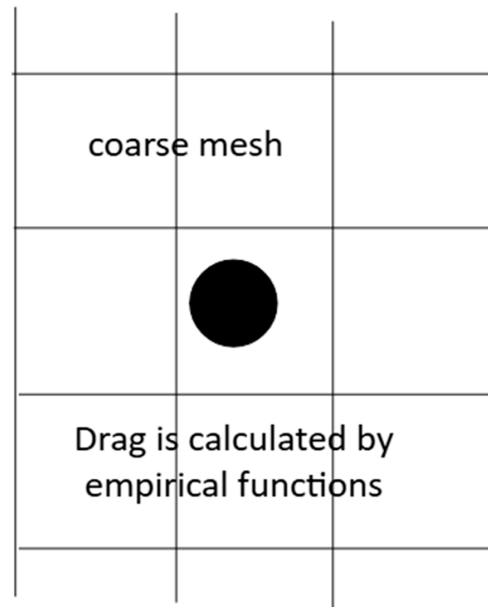


Figure 2. Unresolved CFD-DEM models. The fluid drag force on particles was calculated using empirical models because the coarse mesh sizes were limited to resolve the forces on individual particles.

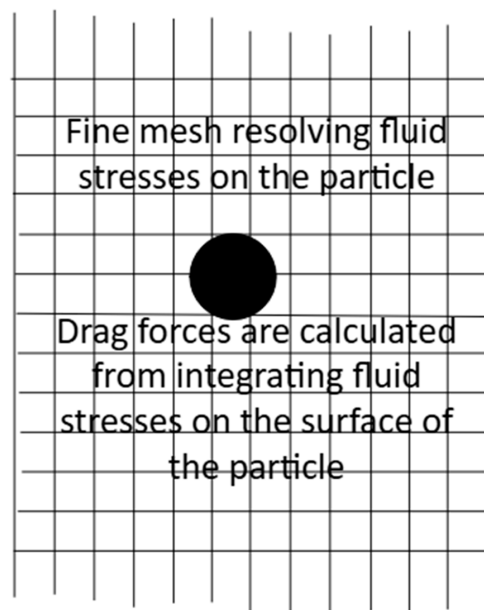


Figure 3. Resolved CFD-DEM models. The fluid drag force on particles was calculated from fluid stresses on the particle surface due to the fine mesh sizes being able to resolve the forces on individual particles.

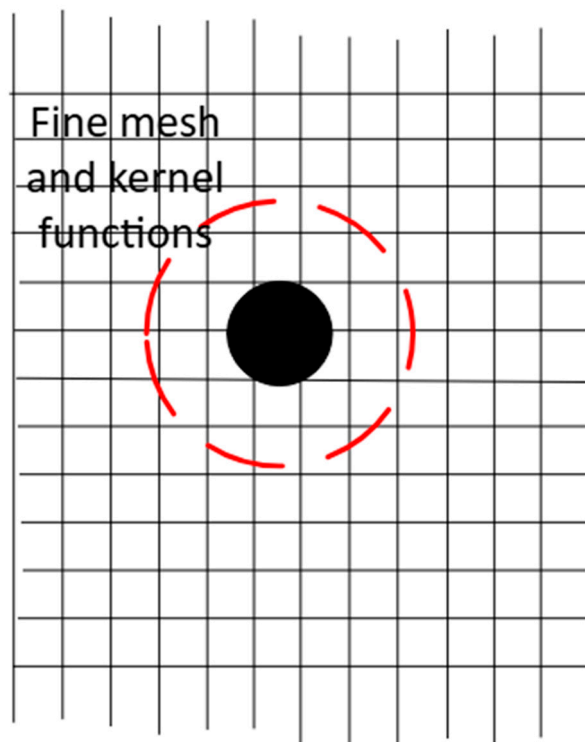


Figure 4. Semi-resolved CFD-DEM models. The fluid drag force on particles was calculated from surrounding meshes using kernel functions. This coupling approach utilizes a kernel function to reconstruct the background information from all cells with centers within a specified smoothing distance, as shown in the red dashed circle, effectively eliminating dependency on grid size. This kernel-based approximation bridges the gap between CFD-DEM simulations using unresolved and resolved meshes, making it highly applicable to particulate flows with finer mesh sizes comparable to or slightly smaller than the particles themselves [92].

2.3. Applications of CFD-DEM in Geotechnical Engineering

Shear stress plays a crucial role in the detachment of soil particles from the surface [94]. When the shear stress exerted by flowing water exceeds the soil's critical shear stress, particles are dislodged and begin to move. The detachment and transport of soil particles depend on several factors, including particle size and distribution, density, and water velocity [95]. Larger and denser particles require more energy to be lifted and transported, while fine particles are more easily carried by flowing water.

In addition to particle size and density, the velocity and turbulence intensity of the water flow directly influence sediment transport mechanisms. High-velocity flows can carry more soil particles, while turbulence enhances particle suspension and transport over longer distances [96]. The interaction between fluid flow and soil properties ultimately determines the extent and severity of erosion, making it essential to understand the underlying dynamics for effective soil conservation practices.

Soil particle transport is often effectively achieved through flow. The underlying mechanism for using flow to dislodge soil particles lies in the formation of a boundary layer near the soil surface. Within this boundary layer, a velocity gradient induces shear stress, which exerts a force on soil particles, rolling them away from their initial positions. For the soil particle to be dislodged, the force generated by the flow must exceed the soil adhesion forces holding it in place.

In laminar flow, the boundary layer is relatively thick, leading to a gradual velocity increase until it reaches the free-stream value. In contrast, turbulent flow is characterized by a thinner boundary layer, which generates substantially higher shear stress. The accurate

prediction of shear stress necessitates a comprehensive understanding of the velocity profiles in both laminar and turbulent flows above the soil surface, as well as the associated boundary layer thickness [97].

Soil particle transport occurs through mechanisms of shearing or rolling under the influence of fluid flow, as shown in Figure 5. The shear force acting on a particle increases with the square of its radius, whereas the frictional force scales linearly with the radius. As a result, there exists a critical particle radius below which the shear force is insufficient to overcome the frictional force, effectively restricting the transport of particles at very small sizes.

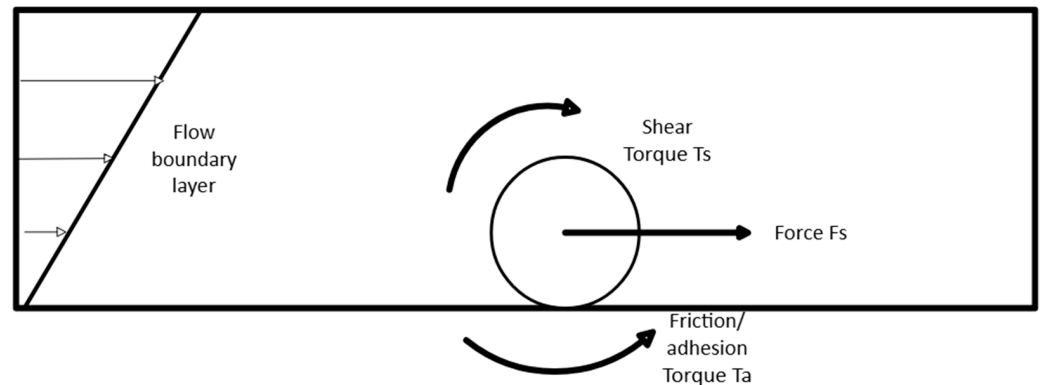


Figure 5. Forces and torques on a soil particle under flow.

In the scenario illustrated in Figure 5, the flow applies a net force component, denoted as F_S to a spherical particle on a surface. This force can drive the particle to slide in a direction parallel to the plane of the surface. Simultaneously, the shear flow creates a torque on the particle, which tends to induce a rolling motion along the surface. However, when the surface is rough, this rolling motion encounters resistance due to adhesion and frictional forces [98].

Studies indicate that the detachment of particles aligns more with the predictions of the rolling mechanism than with those of the sliding mechanism, showing better agreement with observed data [98]. Consequently, it has been concluded that the primary mechanism by which shear flow detaches soil particles is rolling rather than sliding. This rolling-induced detachment under shear flow depends on the critical shear stress needed to overcome the combined effects of surface roughness and adhesion/friction forces acting on the particle [98].

Over the past few years, the application of CFD-DEM has increased rapidly in geotechnical engineering, particularly in the study of multiphase flow systems involving soil particles. In geotechnical engineering, the unresolved CFD-DEM method has been widely used in industries.

Blais et al. [99] reviewed a variety of numerical models, emphasizing the unresolved CFD-DEM approach, which combines CFD for fluid dynamics with the discrete element method (DEM) for solid particles. This method excels in accurately simulating granular dynamics and managing large particle volumes. In their work, Blais et al. extended the unresolved CFD-DEM method to accommodate viscous solid–liquid flows, examining different solid–liquid momentum coupling strategies while comparing their accuracy and stability. They also incorporate a sub-grid viscosity model to maintain accurate suspension rheology.

This refined model is applied to analyze solid–liquid mixing in a stirred tank with a pitched blade turbine. Validation includes qualitative comparisons of particle distribution with experimental data and quantitative measurements of suspended solid fractions using

the pressure gauge technique. Ultimately, this model offers a robust framework for studying and optimizing solid–liquid mixing in laminar and transitional regimes.

The semi-resolved CFD-DEM models have been widely used in geotechnical engineering due to less demand on computational resources and better resolution of particle behaviors. The vertical hydraulic transport of particles with broad size distributions is essential for coal fluidized mining. Wen et al. [90] present a semi-resolved CFD-DEM model to simulate these particle flows, assigning CFD cells as the dependent domain for particle volume and the influential domain for momentum sources. Using a two-way domain expansion for coarse particles and a one-way approach for fine particles, the model introduces dependent and influential domain expansion coefficients to enhance accuracy for coarse particle simulations. Validation through settling and fluidization experiments confirms this model's effectiveness, offering a reliable tool for simulating liquid–solid flows with diverse particle sizes in hydraulic transport applications. Fois et al. [83] introduced a two-dimensional semi-conservative depth-averaged material point method (DAMPM) to simulate flow-like landslides. Governed by shallow-water equations derived from depth-integrated Navier–Stokes equations, the model incorporates bed friction and material rheology using the Voellmy friction model and a depth-integrated Bingham viscoplastic stress model. After validation through benchmark tests, the method was applied to a realistic landslide scenario, highlighting the importance of understanding microscale particle migration in fluid flows for advancing unconventional geo-resources. Zhu et al. [89] enhanced the kernel-based semi-resolved CFD-DEM method with grain-scale reconstruction to study particulate flows in porous materials. A 3D spherical-packed model, derived from the CT images of real rock, captured the heterogeneity and wide grain size distribution of the rock skeleton. Validations showed that the improved semi-resolved CFD-DEM more accurately predicted particle motion, heat transfer, and pressure drop behaviors, closely aligning with experimental and analytical results compared to the unresolved CFD-DEM. Wang et al. [92] identified a simulation gap between resolved CFD-DEM and unresolved CFD-DEM through a study on size effects. They examined the sources of error in conventional unresolved CFD-DEM when simulating particulate flows with comparable mesh sizes and particle diameters. In response, they developed a semi-resolved CFD-DEM model that integrates the strengths of both resolved and unresolved CFD-DEM models. The semi-resolved CFD-DEM employs a drag force model to capture particle–fluid interactions using kernel-based approximations from neighboring fluid cells to correct relative velocity and adjust the void fraction rather than relying solely on the local cell. A Hilbert curve-based search strategy enhances computational efficiency by identifying fluid cells within the kernel's influence area. Numerical simulations comparing various CFD-DEM approaches with experimental data show that the semi-resolved method balances efficiency and accuracy, achieving results comparable to resolved CFD-DEM while maintaining the efficiency of unresolved CFD-DEM. Cheng et al. [93] developed a semi-resolved CFD-DEM model to simulate seepage-induced fine particle migration in gap-graded soils with both fine and coarse particles. The model combines the resolved fictitious domain (FD) method for fluid flow around coarse particles with an unresolved approach based on local averaging for fine particle–fluid interactions. Validated through simple tests, the model was applied to study fine particle migration and piping erosion in gap-graded soils.

The resolved CFD-DEM method, on the other hand, provides a more accurate representation of fluid–particle interactions by fully resolving the flow field around individual particles. Fluid–solid interaction is a crucial scientific issue that draws the attention of researchers in the geological and geotechnical fields, as it is essential for understanding the mechanisms underlying water-induced geohazards in granular soils, such as debris flow, piping erosion, and soil liquefaction. Hu et al. [15] developed a resolved CFD-DEM

coupling method to study fluid–solid interactions and meso-mechanics in granular soils. Validation involved three scenarios, namely the free settling of a single particle, seepage through densely packed particles, and one-dimensional consolidation of a particle column. The effects of mesh size and timestep were analyzed for both dilute and dense systems. Results closely matched experimental and analytical data, capturing nonlinear fluid–solid behaviors such as wake flow, wall effects, and pore-scale dynamics. These findings enhance the understanding of complex interactions in saturated granular soils.

Shen et al. [54] used a resolved coupling model to simulate the interaction between two-phase fluids and irregularly shaped particles using CFD-DEM. The volume of fluid (VoF) method was employed to capture fluid dynamics, while irregular particles were represented as multi-sphere clumps within the DEM framework. This approach calculates meso-scale fluid flow around the particles and proposes an integration scheme to directly compute fluid forces on the multi-sphere particles, eliminating the need for empirical drag force models.

To investigate the movement of soil bodies with arbitrary shapes within a fluid, Mao et al. [53] developed a resolved CFD-DEM coupling algorithm, integrating CFD for the fluid phase with DEM for rigid bodies. The fluid is modeled using Navier–Stokes equations in a Eulerian framework, while rigid body motion follows Newton’s second law in a Lagrangian framework. The immersed boundary method addresses the challenge of representing moving solid boundaries, with interaction forces derived from velocity boundary conditions at the immersed boundary points. Multiple iterations solve the coupling system to capture strong fluid–solid interaction effects.

Kravets et al. [100] compared particle-unresolved CFD-DEM simulations of static homogeneous particle ensembles with DNS using the Lattice Boltzmann method (LBM). By removing particle motion, it focused on assessing CFD accuracy at the particle scale, evaluating drag, lift, and Nusselt numbers. The impact of particle shape on CFD-DEM accuracy was analyzed using spherical, cylindrical, and cubic shapes modeled via the multi-sphere method (MSM). Results highlighted challenges in simulating non-spherical particles and offered insights for improving CFD-DEM applications and closure models.

Estimating the permeability of granular materials like sands is crucial for engineering applications. Permeability is largely influenced by microstructures, particularly in irregular particle configurations. However, the link between the morphological complexity of natural geo-materials and their hydraulic properties has been underexplored. Qi et al. [101] addressed this by developing a workflow combining image processing, the Lattice Boltzmann method (LBM), and the non-spherical discrete element method (DEM). They extracted the geometries of five natural sand particles from micro-CT images, creating monodisperse assemblies with varying porosity using a spheropolyhedra-based DEM. The LBM was then used to analyze pore fluid flow. Results showed that particle shape significantly affects fluid flow, velocity distribution, permeability, tortuosity, and hydraulic anisotropy.

3. Challenges and Knowledge Gaps in CFD-DEM Methods

Despite significant advancements in CFD-DEM methods, challenges persist in achieving a balance between computational efficiency and accuracy. Resolved CFD-DEM offers high accuracy but is computationally intensive due to the requirements for fine mesh sizes and small time steps. Additionally, modeling fluid–solid interactions in large and dense particle systems complicates its application in real-world geotechnical scenarios due to the demand on computational power. However, ongoing research into hybrid approaches, which combine resolved and unresolved CFD-DEM, shows promise for addressing some of these challenges.

A key knowledge gap in both unresolved and resolved CFD-DEM methods is the accurate representation of drag forces and other fluid–solid interaction forces. Unresolved approaches typically rely on empirical drag models, which may not fully capture complex particle-scale behaviors. Resolved CFD-DEM methods employ advanced techniques, such as the fictitious domain (FD) method and the immersed boundary (IB) method, to more precisely model the flow field around particles. However, these techniques also introduce challenges, including the need for mesh reconstruction in systems with deforming particles.

Fluid dynamic mode decomposition models offer a potential new direction to capture soil particle movements. Dynamic mode decomposition models refer to methods used in fluid dynamics and CFD to analyze complex flow fields by breaking them down into simpler modes or structures. These models are part of data-driven analysis techniques that decompose fluid flows into spatial and temporal modes, allowing researchers to study coherent flow structures, turbulence, instabilities, and other dynamic behaviors in a simplified manner. The following are some key models and techniques used for dynamic mode decomposition (DMD) in fluid dynamics:

(1) Proper Orthogonal Decomposition (POD) [102,103]

POD, also known as principal component analysis (PCA) in statistics, is a method for decomposing flow fields into a set of orthogonal modes that capture the most energetic structures in the flow. POD decomposes a set of flow snapshots (data collected over time) into orthogonal spatial modes and corresponding temporal coefficients. The modes are ordered by the amount of energy they contain, so the first few modes represent the most significant flow structures. POD is widely used to analyze turbulence, reduce dimensionality in simulations, and develop low-order models for control in various fluid applications.

(2) Dynamic Mode Decomposition (DMD) [104,105]

DMD is a method for identifying dominant flow structures based on their growth rates and oscillation frequencies. It is particularly useful for analyzing unsteady or time-dependent fluid flows. DMD approximates linear dynamics underlying fluid flows by decomposing time-resolved data into modes that have specific growth/decay rates and frequencies. It uses snapshots of data over time and provides a way to characterize the temporal evolution of the flow. They are used in fluid flow instability studies, turbulence analysis, and developing reduced-order models in complex fluid systems like wake flows and oscillating jets.

(3) Fourier Decomposition [106]

Fourier decomposition breaks down a time-dependent flow into a sum of sinusoidal functions, each with a specific frequency and amplitude, based on Fourier series. This method analyzes the frequency content of the flow and provides insights into periodic and quasi-periodic structures. It can also be used with other decomposition methods to analyze specific frequencies or oscillations. The method is commonly used for flows with periodic behavior, such as vortex shedding or oscillatory flows, where frequency content is crucial.

(4) Global Linear Stability Analysis (GLSA) [107–109]

GLSA studies the stability of fluid flows by decomposing them into modes that describe how small perturbations grow or decay. By linearizing the Navier–Stokes equations around a steady or mean flow, GLSA provides insights into the growth of disturbances in the flow and identifies unstable modes. It is often performed in spectral space. The method is widely used to understand instabilities in boundary layer flows, wake flows, and other flows where small perturbations can lead to significant flow structure changes.

(5) Spectral Proper Orthogonal Decomposition (SPOD) [102,110–112]

SPOD combines POD with Fourier transforms to capture spatial modes that vary over specific frequencies, giving a frequency-resolved analysis of fluid flows. SPOD uses the Fourier transform of the flow data to separate spatial modes by frequency, so each

mode represents coherent structures with a dominant frequency. The method is useful for analyzing coherent structures in turbulent flows, including jets, boundary layers, and wakes, where both the spatial and temporal resolution of flow structures are required.

(6) Koopman Mode Decomposition (KMD) [113,114]

KMD, based on the Koopman operator theory, provides a framework for nonlinear flow analysis by decomposing the flow into modes associated with a continuous spectrum of frequencies. Unlike DMD, which approximates linear dynamics, KMD considers the full nonlinear dynamics of the flow. It is especially useful in analyzing nonlinear systems, as it provides modes with interpretable dynamics even for complex systems. The method is used in complex nonlinear flow systems and dynamical systems to uncover recurrent patterns and structures in turbulent flows.

(7) Balanced Proper Orthogonal Decomposition (BPOD) [115,116]

BPOD is a modification of POD that specifically focuses on decomposing flows with an emphasis on input–output behavior, often used for flow control applications. BPOD modifies the standard POD approach by balancing the modes based on their controllability and observability, which makes it useful in control and systematic analysis. The BPOD model is commonly applied in flow control, where understanding how inputs affect the system response is important, such as in drag reduction or boundary layer control.

(8) Resolvent Analysis [117–120]

Resolvent analysis examines the response of a fluid system to external forcing and decomposes the flow field into forcing and response modes. This method uses the resolvent operator, which is derived from the Navier–Stokes equations, to identify which flow structures are most amplified by the system’s inherent dynamics. The method is useful in turbulent flow analysis and in understanding which disturbances are likely to be amplified, such as in jets or boundary layers. It also aids in predicting coherent structures in turbulent flows.

(9) Wavelet Decomposition [121,122]

Wavelet decomposition analyzes the flow using localized functions that can capture both frequency and spatial information, making it ideal for analyzing transient and non-periodic flows. The wavelet transform breaks down flow data into wavelets with specific frequencies and spatial locations. Unlike Fourier transforms, wavelets can capture short-lived and localized events within the flow. The model is used for analyzing unsteady and transient events, such as turbulence, flow separation, and vortex interactions, where local flow dynamics are important.

(10) Empirical Mode Decomposition (EMD) [123,124]

EMD decomposes a flow field into intrinsic mode functions (IMFs) based on the flow’s data structure, without assuming a specific basis function. EMD is a data-driven approach that iteratively extracts IMFs, each representing a specific oscillatory mode. It is particularly suited to nonlinear and nonstationary flows. The method is useful for analyzing complex unsteady flows that exhibit nonlinear behavior, such as vortex-dominated flows or flows with intermittent instabilities.

Benefits and Applications of Fluid Dynamic Mode Decomposition Models:

Turbulence analysis: DMD, POD, and SPOD help in breaking down turbulent flows into dominant structures, aiding in understanding turbulence energy transfer and coherent structures.

Flow control: models like BPOD are applied in developing control strategies by focusing on dominant controllable modes in the flow.

Reduced-order modeling: DMD and POD allow for constructing reduced-order models, simplifying complex fluid systems for real-time applications like simulations, design, and control.

Instability studies: decomposition models reveal flow instabilities, providing insights into phenomena such as vortex shedding, boundary layer separation, and transitions to turbulence.

Machine learning integration: decomposition methods, such as POD and DMD, provide low-dimensional representations, which can be integrated with machine learning algorithms for predictive modeling and anomaly detection in fluid systems.

Fluid dynamic mode decomposition models play a crucial role in simplifying, understanding, and controlling fluid flows, particularly in complex and turbulent systems. Each method has unique strengths suited to specific applications, ranging from flow stability analysis and turbulence to reduced-order modeling and flow control.

Since soil particles behave as dynamic systems governed by Newton's second law, integrating fluid dynamic mode models into particle dynamics systems is a natural and promising approach. This integration allows for a more comprehensive simulation of fluid–solid interactions, capturing both the forces on individual particles and the complex fluid flow around them. Conducting a thorough review of the current state of dynamic systems and their modeling techniques can help address knowledge gaps and provide valuable insights into the behavior of these particle–fluid systems. Such an analysis can also help identify areas where these systems may be further optimized, offering alternative approaches to improve the computational solvability of complex dynamic modes in fluid–particle simulations. This method not only enhances model accuracy but also supports the development of computational strategies that make large-scale simulations of particulate flows more feasible and effective.

Another promising approach in fluid–particle simulations is the integration of LBM-DEM models [101,125,126]. Fluid Lattice Boltzmann models (LBMs) are computational fluid dynamics (CFD) techniques, based on the Lattice Boltzmann method, which simulate fluid flow by modeling it as particles distributed across a lattice grid. Unlike traditional CFD approaches that directly solve the Navier–Stokes equations, the LBM captures fluid dynamics by evolving particle distribution functions through collision and propagation rules on the lattice. This approach enables the LBM to capture fluid behaviors on both macroscopic and microscopic scales, making it particularly useful for simulating complex and dynamic fluid systems.

The following are some key features and advantages of fluid LBM models:

Discrete lattice structure: Fluid is represented on a discrete lattice, with particles moving between grid points. The lattice structure and spacing can vary based on the application, often chosen to balance accuracy and computational efficiency.

Microscopic-based approach: The LBM is based on kinetic theory and simulates fluid flow by updating the probability distribution of fluid particles on the lattice. This mesoscopic approach bridges the gap between macroscopic and microscopic perspectives.

Collision and streaming process: At each time step, particles collide and redistribute their velocities (collision), then move or “stream” to neighboring lattice points. The collision model, such as the BGK (Bhatnagar–Gross–Krook) model, is a simplified approach to handle particle interactions and drive the system toward equilibrium.

Boundary conditions: LBM models are flexible in handling complex boundary conditions, including solid boundaries, moving interfaces, and even multiphase boundaries, which makes them well-suited for simulating porous media, fluid–particle flows, and flows with complex geometries.

Advantages in complex geometries and multiphase flow: The LBM is often preferred in applications like porous media flow, multiphase flows, fluid–particle interactions, and turbulent flows because it can handle these situations more naturally than traditional CFD methods. It also works well for flows with complex boundary interactions and interface

dynamics, like those encountered in biological or geological systems, such as lubricating between porous cartilage tissues [127].

Parallelization: The LBM is highly parallelizable due to its local interactions, which makes it efficient on modern high-performance computing platforms, enabling simulations of large complex systems.

Types of LBM Models for Fluid Dynamics:

Single-phase models: standard LBM models that simulate single-phase fluid flows, used widely for incompressible or weakly compressible flows.

Multiphase and multicomponent models: The LBM has specialized models for simulating multiphase (e.g., liquid–gas) and multicomponent (e.g., fluid–fluid) systems. These include models like the Shan Chen model for attractive–repulsive interactions.

Thermal LBM models: these include energy equations to model thermal flows, accounting for temperature variations and heat transfer, useful in thermal fluid dynamics.

In summary, fluid LBM models are powerful tools in CFD, offering a unique approach for simulating complex flows with advantages in flexibility, scalability, and computational efficiency.

4. Future Directions and Conclusions

The future of CFD-DEM modeling in geotechnical engineering lies in improving computational efficiency while maintaining accuracy, particularly for large-scale real-world applications. Advances in hybrid modeling techniques, such as coupling resolved and unresolved CFD-DEM, LBM-CFD, and dynamic mode decomposition models offer promising solutions for balancing these demands. Additionally, further research into the effects of particle shape, pore-scale interactions, and drag force models will help refine the accuracy of these simulations.

Artificial intelligence (AI) has transformed soil erosion analysis by introducing advanced machine learning data-driven methods [11,26,33,105,128]. It is projected that machine learning (ML) and deep learning (DL) algorithms and their roles in accurately assessing soil erosion are increasingly more important [128]. We need to explore how AI leverages historical data, remote sensing imagery, and various geospatial datasets to improve erosion quantification. The AI-based models emphasize the impact of AI-driven methodologies on addressing complex erosion issues, including large-scale fluid–soil interactions, enhancing predictive models, and supporting informed decision-making. Integrating AI in soil erosion analysis offers substantial benefits for sustainable land management by providing decision-makers with actionable insights to optimize agricultural practices, reduce erosion risks, and promote ecologically responsible land use.

As computational power continues to grow, the CFD-DEM and AI method is expected to play an increasingly important role in understanding fluid–solid interactions in granular soils. By providing detailed insights into processes such as seepage, liquefaction, and sediment transport, CFD-DEM and AI methods will be essential in developing better strategies for managing geotechnical hazards and soil erosion in the following areas:

Soil conservation: insights into erosion processes aid in developing effective conservation strategies like terraces, contour plowing, and vegetative cover.

Water quality: managing erosion reduces sedimentation in water bodies, improving water quality and aquatic habitats.

Agricultural productivity: erosion control measures are essential for maintaining soil fertility and agricultural productivity.

Infrastructure protection: hydrodynamic studies assist in designing structures to protect infrastructure from erosion damage.

This review highlights the current state of CFD-DEM methods in fluid–solid interaction and their applications in geotechnical engineering, emphasizing the importance of continued research to improve the accuracy and efficiency of these numerical simulations for practical applications.

Author Contributions: J.X. wrote the paper and F.W. and R.A. edited the paper. All authors contributed equally. All authors have read and agreed to the published version of the manuscript.

Funding: This research was funded by the Postdoctoral Research Scholar Program offered by the Provost of Tarleton State University.

Conflicts of Interest: There are no conflicts of interest.

References

1. Borrelli, P.; Alewell, C.; Alvarez, P.; Anache, J.A.A.; Baartman, J.; Ballabio, C.; Bezak, N.; Biddoccu, M.; Cerdà, A.; Chalise, D.; et al. Soil erosion modelling: A global review and statistical analysis. *Sci. Total Environ.* **2021**, *780*, 146494. [[CrossRef](#)] [[PubMed](#)]
2. Koch, T.; Chiffard, P.; Aartsma, P.; Panten, K. A review of the characteristics of rainfall simulators in soil erosion research studies. *Methodsx* **2024**, *12*, 102506. [[CrossRef](#)]
3. Wang, D.D.; Yuan, Z.J.; Cai, Y.T.; Jing, D.W.; Liu, F.; Tang, Y.; Song, N.N.; Li, Y.Y.; Zhao, C.Y.; Fu, X.Y. Characterisation of soil erosion and overland flow on vegetation-growing slopes in fragile ecological regions: A review. *J. Environ. Manag.* **2021**, *285*, 112165. [[CrossRef](#)] [[PubMed](#)]
4. Chen, S.C.; Chou, H.T.; Chen, S.C.; Wu, C.H.; Lin, B.S. Characteristics of rainfall-induced landslides in Miocene formations: A case study of the Shenmu watershed, Central Taiwan. *Eng. Geol.* **2014**, *169*, 133–146. [[CrossRef](#)]
5. Pimentel, D.; Harvey, C.; Resosudarmo, P.; Sinclair, K.; Kurz, D.; Mcnair, M.; Crist, S.; Shpritz, L.; Fitton, L.; Saffouri, R.; et al. Environmental and Economic Costs of Soil Erosion and Conservation Benefits. *Science* **1995**, *267*, 1117–1123. [[CrossRef](#)] [[PubMed](#)]
6. Liu, L.; Li, Z.W.; Li, Z.J.; Liu, E.F.; Nie, X.D.; Liu, C.; Xiao, H.B. Effect of aggregate breakdown on the unevenly enriched organic carbon process in sediments under a rain-induced overland flow. *Soil Tillage Res.* **2020**, *204*, 104752. [[CrossRef](#)]
7. Ma, D.; Duan, H.Y.; Li, X.B.; Li, Z.H.; Zhou, Z.L.; Li, T.B. Effects of seepage-induced erosion on nonlinear hydraulic properties of broken red sandstones. *Tunn. Undergr. Space Tech.* **2019**, *91*, 102993. [[CrossRef](#)]
8. Borrelli, P.; Robinson, D.A.; Panagos, P.; Lugato, E.; Yang, J.E.; Alewell, C.; Wuepper, D.; Montanarella, L.; Ballabio, C. Land use and climate change impacts on global soil erosion by water (2015–2070). *Proc. Natl. Acad. Sci. USA* **2020**, *117*, 21994–22001. [[CrossRef](#)] [[PubMed](#)]
9. Li, X.Y.; Fan, H.H.; Xie, F.H.; Lei, B.F.; Ren, G.Z. The role of soil dispersivity and initial moisture content in splash erosion: Findings from consecutive single-drop splash tests. *Biosyst. Eng.* **2024**, *243*, 27–41. [[CrossRef](#)]
10. Mohebzadeh, H.; Biswas, A.; DeVries, B.; Rudra, R.; Shukla, R.; Daggupati, P. Evaluation of the impact of best management practices on ephemeral gully and sheet/rill erosion using the AnnAGNPS model. *Catena* **2024**, *246*, 108436. [[CrossRef](#)]
11. Gao, R.L.; Gao, M.F.; Yao, S.H.; Wen, Y.R. Gully erosion susceptibility mapping considering seasonal variations of NDVI using a machine learning approach in the Mollisol region of China. *Soil Tillage Res.* **2025**, *245*, 106322. [[CrossRef](#)]
12. Molina, N.; Walczak, M.; Kalbarczyk, M.; Celentano, D. Erosion under turbulent slurry flow: Effect of particle size in determining impact velocity and wear correlation by inverse analysis. *Wear* **2021**, *474*, 203651. [[CrossRef](#)]
13. Sedano-de la Rosa, C.; Vite-Torres, M.; Gallardo-Hernández, E.A.; Laguna-Camacho, J.R.; Godínez-Salcedo, J.G.; Farfán-Cabrera, L.I. Effect of tangential velocity on erosion of ASTM A-106 Grade B steel pipe under turbulent swirling impinging jet. *Tribol. Int.* **2017**, *113*, 500–506. [[CrossRef](#)]
14. Chao, H.; Tan, Y.; Su, Z.K. Ground failure and soil erosion caused by bursting of buried water pipeline: Experimental and numerical investigations. *Eng. Fail. Anal.* **2025**, *167*, 108965. [[CrossRef](#)]
15. Hu, G.Y.; Zhou, B.; Yang, B.; Wang, H.B.; Liu, Z.J. An insight into the interaction between fluid and granular soil based on a resolved CFD-DEM method. *Comput. Geo.* **2023**, *163*, 105722. [[CrossRef](#)]
16. Li, X.; Ren, J.Q.; Xue, J.L.; Xu, Q.X.; Yuan, J.; Zhang, W. Interpretation of delayed suspended sediment transport during flood events from the perspective of movement characteristics. *J. Hydrol.* **2024**, *644*, 132127. [[CrossRef](#)]
17. OuYang, H.R.; Dai, G.L.; Gao, L.C.; Zhu, W.B.; Du, S.; Gong, W.M. Local scour characteristics of monopile foundation and scour protection of cement-improved soil in marine environment-Laboratory and site investigation. *Ocean Eng.* **2022**, *255*, 111443. [[CrossRef](#)]
18. Chen, C.; Zhang, P.T.; Zhang, L.M.; Zhang, J.M.; Xue, J.H.; Lu, H. Internal erosion in granular soils with different microstructures under cyclically increased hydraulic gradients. *J. Hydrol.* **2024**, *639*, 131601. [[CrossRef](#)]

19. Hu, J.; Xiao, Y.; Shi, J.Q.; Stuedlein, A.W.; Evans, T.M. Small-strain shear strain and liquefaction resistance of sand. *Geotechnique* **2024**, *1*–14. [[CrossRef](#)]
20. Baggio, T.; Martini, M.; Bettella, F.; D'Agostino, V. Debris flow and debris flood hazard assessment in mountain catchments. *Catena* **2024**, *245*, 108338. [[CrossRef](#)]
21. Zhang, F.; Damjanac, B.; Furtney, J. *Coupled Thermo-Hydro-Mechanical Processes in Fractured Rock Masses: Discrete Element Modeling and Engineering Applications*; Springer: Berlin/Heidelberg, Germany, 2023.
22. Wang, C.H.; Xu, C.X. Direct numerical simulation of a supersonic turbulent boundary layer with hydrogen combustion. *J. Fluid Mech.* **2024**, *998*, A1. [[CrossRef](#)]
23. Wang, Y.X.; Li, C.Y.; Peng, D.Z.; Tse, T.K.T. Direct numerical simulation of sand particles transporting in the atmospheric Ekman boundary layer. *Flow* **2024**, *4*, E22. [[CrossRef](#)]
24. Glowinski, R.; Pan, T.W.; Hesla, T.I.; Joseph, D.D.; Périaux, J. A fictitious domain approach to the direct numerical simulation of incompressible viscous flow past moving rigid bodies: Application to particulate flow. *J. Comput. Phys.* **2001**, *169*, 363–426. [[CrossRef](#)]
25. Dou, J.X.; Wang, L.M.; Ge, W. Particle-resolved direct numerical simulation and bottom-up statistical analysis on solid-phase pressure in particle-fluid systems. *Chem. Eng. J.* **2024**, *499*, 156312. [[CrossRef](#)]
26. Fatahian, H.; Mishra, R.; Jackson, F.F.; Fatahian, E. Data-driven multi-objective optimization of aerodynamics and aeroacoustics in dual Savonius wind turbines using large eddy simulation and machine learning. *Phys. Fluids* **2024**, *36*, 105176. [[CrossRef](#)]
27. Mou, C.Q.; Che, B.X.; Wang, Y.X.; Zhang, J.S.; Cao, L.L.; Wu, D.Z. Large eddy simulation of micro vortex generator-controlled cavitation across multiple stages. *Phys. Fluids* **2024**, *36*, 104115. [[CrossRef](#)]
28. Theja, C.; Sathia, K.R.; Mahesh, S.; Narasimhamurthy, V.D. Large eddy simulation of turbulent wake from dual-step cylinders. *Phys. Fluids* **2024**, *36*, 105163. [[CrossRef](#)]
29. Zhang, H.; Hu, H.B.; Zhang, F.; Chen, X.P. Subgrid-scale model for large eddy simulations of incompressible turbulent flows within the lattice Boltzmann framework. *Phys. Rev. E* **2024**, *110*, 045305. [[CrossRef](#)] [[PubMed](#)]
30. Kumar, A.A.; Assam, A. Addressing performance improvement of a neural network model for Reynolds-averaged Navier-Stokes solutions with high wake formation. *Eng. Comput.* **2024**, *41*, 1740–1765. [[CrossRef](#)]
31. Bhattarai, B.; Hilliard, B.; Tonina, D.; Reeder, W.J.; Budwig, R.; Martin, B.T.; Xing, T. Evaluation of Reynolds-averaged Navier-Stokes turbulence models in open channel flow over salmon redds. *J. Hydrodyn.* **2024**, *36*, 741–756. [[CrossRef](#)]
32. Hu, K.S.; Shih, T.I.P. Large-Eddy vs. Reynolds-Averaged Navier-Stokes Simulations of Flow and Heat Transfer in a U-Duct with Unsteady Flow Separation. *Energies* **2024**, *17*, 2414. [[CrossRef](#)]
33. Zhang, X.C.; Zhang, Z.; Chinnici, A.; Sun, Z.W.; Shi, J.Q.; Nathan, G.J.; Chin, R.C. Physics-informed data-driven unsteady Reynolds-averaged Navier-Stokes turbulence modeling for particle-laden jet flows. *Phys. Fluids* **2024**, *36*, 053325. [[CrossRef](#)]
34. Joo, D.; You, D. A Reynolds-averaged Navier-Stokes closure for steady-state simulations of Rayleigh-Benard convection. *Phys. Fluids* **2024**, *36*, 085154. [[CrossRef](#)]
35. Syawitri, T.P.; Yao, Y.F.; Chandra, B.; Yao, J. Comparison study of URANS and hybrid RANS-LES models on predicting vertical axis wind turbine performance at low, medium and high tip speed ratio ranges. *Renew. Energ.* **2021**, *168*, 247–269. [[CrossRef](#)]
36. Haering, S.W.; Oliver, T.A.; Moser, R.D. Active model split hybrid RANS/LES. *Phys. Rev. Fluids* **2022**, *7*, 014603. [[CrossRef](#)]
37. Mays, M.D.; Lardeau, S.; Laizet, S. Capturing the drag crisis in the flow around a smooth cylinder using a hybrid RANS-LES model on coarse meshes. *Int. J. Heat Fluid Flow* **2023**, *103*, 109203. [[CrossRef](#)]
38. Menter, F.; Hüppe, A.; Matyushenko, A.; Kolmogorov, D. An Overview of Hybrid RANS-LES Models Developed for Industrial CFD. *Appl. Sci.* **2021**, *11*, 2459. [[CrossRef](#)]
39. Wang, A.; Yang, X.I.A.; Ovchinnikov, M. An Investigation of LES Wall Modeling for Rayleigh-Benard Convection via Interpretable and Physics-Aware Feedforward Neural Networks with DNS. *J. Atmos. Sci.* **2024**, *81*, 435–458.
40. Iousef, S.; Montazeri, H.; Blocken, B.; van Wesemael, P.J.V. Wall-resolved versus wall-modeled LES of the flow field and surface forced convective heat transfer for a low-rise building. *Build. Environ.* **2023**, *244*, 110678. [[CrossRef](#)]
41. Liefvendahl, M.; Johansson, M. Wall-Modeled LES for Ship Hydrodynamics in Model Scale. *J. Ship. Res.* **2021**, *65*, 41–54. [[CrossRef](#)]
42. Iphineni, H.; Windén, B.; Girimaji, S.S. Toward high-fidelity Numerical Wave Tank development: Scale resolving Partially-Averaged Navier-Stokes simulations of dam-break flow. *Ocean. Eng.* **2024**, *291*, 116407. [[CrossRef](#)]
43. Wang, X.L.; Wang, Y.; Yuan, X.; Liu, H.L.; Jiang, L.L.; Xiong, W. Numerical investigation of cavitating flow in centrifugal pump with improved partially-averaged Navier-Stokes method. *J. Hydraul. Res.* **2023**, *61*, 809–823. [[CrossRef](#)]
44. Dzanic, T.; Girimaji, S.S.; Witherden, F.D. Partially-averaged Navier-Stokes simulations of turbulence within a high-order flux reconstruction framework. *J. Comput. Phys.* **2022**, *456*, 110992. [[CrossRef](#)]
45. Fowler, T.S.; Witherden, F.D.; Girimaji, S.S. Partially-averaged Navier-Stokes simulations of turbulent flow past a square cylinder: Comparative assessment of statistics and coherent structures at different resolutions. *Phys. Fluids* **2020**, *32*, 125106. [[CrossRef](#)]

46. Sun, X.; Sakai, M.; Yamada, Y. Three-dimensional simulation of a solid-liquid flow by the DEM-SPH method. *J. Comput. Phys.* **2013**, *248*, 147–176. [[CrossRef](#)]
47. Goldman, A.J.; Cox, R.G.; Brenner, H. Slow Viscous Motion of a Sphere Parallel to a Plane Wall—II Couette Flow. *Chem. Eng. Sci.* **1967**, *22*, 653–660. [[CrossRef](#)]
48. Feng, R.F.; Fourtakas, G.; Rogers, B.D.; Lombardi, D. Modelling internal erosion using 2D smoothed particle hydrodynamics (SPH). *J. Hydrol.* **2024**, *639*, 131558. [[CrossRef](#)]
49. Hoomans, B.P.B.; Kuipers, J.A.M.; Briels, W.J.; vanSwaaij, W.P.M. Discrete particle simulation of bubble and slug formation in a two-dimensional gas-fluidised bed: A hard-sphere approach. *Chem. Eng. Sci.* **1996**, *51*, 99–118. [[CrossRef](#)]
50. Hu, Z.; Zhang, Y.D.; Yang, Z.X. Suffusion-induced deformation and microstructural change of granular soils: A coupled CFD-DEM study. *Acta Geotech.* **2019**, *14*, 795–814. [[CrossRef](#)]
51. Jiang, M.J.; Sun, C.; Crosta, G.B.; Zhang, W.C. A study of submarine steep slope failures triggered by thermal dissociation of methane hydrates using a coupled CFD-DEM approach. *Eng. Geol.* **2015**, *190*, 1–16. [[CrossRef](#)]
52. Sun, R.; Xiao, H. SediFoam: A general-purpose, open-source CFD-DEM solver for particle-laden flow with emphasis on sediment transport. *Comput. Geosci.* **2016**, *89*, 207–219. [[CrossRef](#)]
53. Mao, J.; Zhao, L.H.; Liu, X.N.; Di, Y.T. A resolved CFDEM algorithm based on the immersed boundary for the simulation of fluid-solid interaction. *Powder Technol.* **2020**, *374*, 290–303. [[CrossRef](#)]
54. Shen, Z.H.; Wang, G.; Huang, D.R.; Jin, F. A resolved CFD-DEM coupling model for modeling two-phase fluids interaction with irregularly shaped particles. *J. Comput. Phys.* **2022**, *448*, 110695. [[CrossRef](#)]
55. Tao, H.; Tao, J.L. Quantitative analysis of piping erosion micro-mechanisms with coupled CFD and DEM method. *Acta Geotech.* **2017**, *12*, 573–592. [[CrossRef](#)]
56. Bao, X.H.; Wu, H.; Xiong, H.; Chen, X.S. Particle shape effects on submarine landslides via CFD-DEM. *Ocean. Eng.* **2023**, *284*, 115140. [[CrossRef](#)]
57. Sun, J.Q.; Li, X.A.; Li, J.; Zhang, J.; Zhang, Y.T. Numerical investigation of characteristics and mechanism of tunnel erosion of loess with coupled CFD and DEM method. *Catena* **2023**, *222*, 106729. [[CrossRef](#)]
58. Cui, Y.F.; Nouri, A.; Chan, D.; Rahmati, E. A new approach to DEM simulation of sand production. *J. Pet. Sci. Eng.* **2016**, *147*, 56–67. [[CrossRef](#)]
59. Nian, T.K.; Li, D.Y.; Liang, Q.H.; Wu, H.; Guo, X.S. Multi-phase flow simulation of landslide dam formation process based on extended coupled DEM-CFD method. *Comput. Geotech.* **2021**, *140*, 104438. [[CrossRef](#)]
60. Teng, P.H.; Johansson, F.; Hellström, J.G.I. Modelling erosion of a single rock block using a coupled CFD-DEM approach. *J. Rock Mech. Geotech.* **2023**, *15*, 2375–2387. [[CrossRef](#)]
61. Wang, Y.; Cheng, K.; Yang, Y.F.; Tao, Y.C.; Li, Y.W. Microscopic mechanical analysis of sand production using a new arbitrary resolved-unresolved CFD-DEM model. *Int. J. Multiph. Flow* **2022**, *149*, 103979. [[CrossRef](#)]
62. Peng, Y.; Yin, Z.Y.; Zhou, C.; Ding, X.M. Micromechanical analysis of capillary suction effect on bearing capacity of unsaturated fine granular foundation soil using coupled CFD-DEM method. *Comput. Geotech.* **2023**, *153*, 105092. [[CrossRef](#)]
63. Qian, J.G.; Zhou, C.; Yin, Z.Y.; Li, W.Y. Investigating the effect of particle angularity on suffusion of gap-graded soil using coupled CFD-DEM. *Comput. Geotech.* **2021**, *139*, 104383. [[CrossRef](#)]
64. Qian, J.G.; Li, W.Y.; Yin, Z.Y.; Yang, Y. Influences of buried depth and grain size distribution on seepage erosion in granular soils around tunnel by coupled CFD-DEM approach. *Transp. Geotech.* **2021**, *29*, 100574. [[CrossRef](#)]
65. Guo, Y.; Yang, Y.; Yu, X. Influence of particle shape on the erodibility of non-cohesive soil: Insights from coupled CFD-DEM simulations. *Particuology* **2018**, *39*, 12–24. [[CrossRef](#)]
66. Cheng, Y.; Wang, T.; Wang, P.; Qin, S.; Zhou, W.H.; Yin, Z.Y. Hydromechanical analysis of slurry infiltration with coupled CFD-DEM method. *Int. J. Numer. Anal. Methods Geomech.* **2024**, *48*, 3032–3053. [[CrossRef](#)]
67. Rahimi-Larki, M.; Vollmann, S.; Jin, S.L. Flow-induced erosion modelling of cohesive material with coupled CFD-DEM approach. *Miner. Eng.* **2024**, *217*, 108947. [[CrossRef](#)]
68. Jing, L.; Kwok, C.Y.; Leung, Y.F.; Sobral, Y.D. Extended CFD-DEM for free-surface flow with multi-size granules. *Int. J. Numer. Anal. Methods Geomech.* **2016**, *40*, 62–79. [[CrossRef](#)]
69. Börner, M.; Bück, A.; Tsotsas, E. DEM-CFD investigation of particle residence time distribution in top-spray fluidised bed granulation. *Chem. Eng. Sci.* **2017**, *161*, 187–197. [[CrossRef](#)]
70. Iqbal, N.; Rauh, C. Coupling of discrete element model (DEM) with computational fluid mechanics (CFD): A validation study. *Appl. Math. Comput.* **2016**, *277*, 154–163. [[CrossRef](#)]
71. Zhao, J.D.; Shan, T. Coupled CFD-DEM simulation of fluid-particle interaction in geomechanics. *Powder Technol.* **2013**, *239*, 248–258. [[CrossRef](#)]
72. Mu, L.L.; Zhang, P.Y.; Shi, Z.H.; Huang, M.S. Coupled CFD-DEM Investigation of Erosion Accompanied by Clogging Mechanism under Different Hydraulic Gradients. *Comput. Geotech.* **2023**, *153*, 105058. [[CrossRef](#)]

73. Zhang, P.Y.; Mu, L.L.; Huang, M.S. A coupled CFD-DEM investigation into hydro-mechanical behaviour of gap-graded soil experiencing seepage erosion considering cyclic hydraulic loading. *J. Hydrol.* **2023**, *624*, 129908. [[CrossRef](#)]
74. Guo, Y.; Yu, X. Comparison of the implementation of three common types of coupled CFD-DEM model for simulating soil surface erosion. *Int. J. Multiph. Flow* **2017**, *91*, 89–100. [[CrossRef](#)]
75. Guo, Y.; Xiao, J.Q.; Wang, C. A coarse graining CFD-DEM simulation on contact erosion of layered cohesionless soils. *Can. Geotech. J.* **2024**, *61*, 534–548. [[CrossRef](#)]
76. Kuang, S.B.; Zhou, M.M.; Yu, A.B. CFD-DEM modelling and simulation of pneumatic conveying: A review. *Powder Technol.* **2020**, *365*, 186–207. [[CrossRef](#)]
77. Zhang, D.M.; Gao, C.P.; Yin, Z.Y. CFD-DEM modeling of seepage erosion around shield tunnels. *Tunn. Undergr. Space Tech.* **2019**, *83*, 60–72. [[CrossRef](#)]
78. Guo, Y.; Yu, X. Analysis of surface erosion of cohesionless soils using a three-dimensional coupled computational fluid dynamics—Discrete element method (CFD-DEM) model. *Can. Geotech. J.* **2019**, *56*, 687–698. [[CrossRef](#)]
79. Xiao, H.; Sun, J. Algorithms in a Robust Hybrid CFD-DEM Solver for Particle-Laden Flows. *Commun. Comput. Phys.* **2011**, *9*, 297–323. [[CrossRef](#)]
80. Cundall, P.A.; Strack, O.D.L. A Discrete Numerical-Model for Granular Assemblies—Reply. *Geotechnique* **1980**, *30*, 335–336. [[CrossRef](#)]
81. Bisht, V.; Salgado, R.; Prezzi, M. Simulation of cone penetration in soil using the material point method. *Comput. Geotech.* **2024**, *172*, 106430. [[CrossRef](#)]
82. Ceccato, F.; Yerro, A.; Di Carluccio, G. Simulating landslides with the material point method: Best practices, potentialities, and challenges. *Eng. Geol.* **2024**, *338*, 107614. [[CrossRef](#)]
83. Fois, M.; de Falco, C.; Formaggia, L. A semi-conservative depth-averaged material point method for fast flow-like landslides and mudflows. *Commun. Nonlinear Sci. Numer. Simul.* **2024**, *138*, 108202. [[CrossRef](#)]
84. Urmi, Z.A.; Yerro, A.; Saeidi, A.; Chavali, R.V.P. Prediction of retrogressive landslide in sensitive clays by incorporating a novel strain softening law into the Material Point Method. *Eng. Geol.* **2024**, *340*, 107669. [[CrossRef](#)]
85. Acosta, J.L.G.; Mánica, M.A.; Vardon, P.J.; Hicks, M.A.; Gens, A. A nonlocal material point method for the simulation of large deformation problems in brittle soils. *Comput. Geotech.* **2024**, *172*, 106424. [[CrossRef](#)]
86. Chandra, B.; Hashimoto, R.; Kamrin, K.; Soga, K. Mixed material point method formulation, stabilization, and validation for a unified analysis of free-surface and seepage flow. *J. Comput. Phys.* **2024**, *519*, 113457. [[CrossRef](#)]
87. Kontoe, M.; Lopez-Querol, S.; Rossetto, T. Application of the material point method (MPM) to characterise the impact forces of granular landslides on rigid obstacles. *Soil Dyn. Earthq. Eng.* **2024**, *184*, 108726. [[CrossRef](#)]
88. Kloss, C.; Goniva, C.; Hager, A.; Amberger, S.; Pirker, S. Models, algorithms and validation for opensource DEM and CFD-DEM. *Prog. Comput. Fluid Dyn. Int. J.* **2012**, *12*, 140–152. [[CrossRef](#)]
89. Zhu, G.P.; Zhao, Y.X.; Wang, Z.K.; Khalid, M.S.U.; Liu, M.B. Semi-resolved CFD-DEM simulation of fine particle migration with heat transfer in heterogeneous porous media. *Int. J. Heat Mass Tran.* **2022**, *197*, 123349. [[CrossRef](#)]
90. Wen, X.J.; Zheng, L.N.; Zhao, X.; Liu, Y.K.; Kang, J.H.; Ye, G.Q.; Wang, F.C.; Yuan, M.; Jiang, M.J. An improved semi-resolved computational fluid dynamics-discrete element method for simulating liquid-solid systems with wide particle size distributions. *Phys. Fluids* **2024**, *36*, 033343. [[CrossRef](#)]
91. Wang, Z.K.; Liu, M.B. Semi-resolved CFD-DEM for thermal particulate flows with applications to fluidized beds. *Int. J. Heat Mass Tran.* **2020**, *159*, 12015. [[CrossRef](#)]
92. Wang, Z.K.; Teng, Y.J.; Liu, M.B. A semi-resolved CFD-DEM approach for particulate flows with kernel based approximation and Hilbert curve based searching strategy. *J. Comput. Phys.* **2019**, *384*, 151–169. [[CrossRef](#)]
93. Cheng, K.; Wang, Y.; Yang, Q. A semi-resolved CFD-DEM model for seepage-induced fine particle migration in gap-graded soils. *Comput. Geotech.* **2018**, *100*, 30–51. [[CrossRef](#)]
94. Li, Z.C.; Hua, J.; Yin, P.F.; Zhang, H. Shear failure analysis of slip zone soil with different coarse particle shapes: Visualized shear test and PIV technology. *Eng. Fail. Anal.* **2024**, *162*, 108345. [[CrossRef](#)]
95. Li, W.; Brunetti, G.; Zafiu, C.; Kunaschk, M.; Debreczeby, M.; Stumpp, C. Experimental and simulated microplastics transport in saturated natural sediments: Impact of grain size and particle size. *J. Hazard. Mater.* **2024**, *468*, 133772. [[CrossRef](#)] [[PubMed](#)]
96. Sommerfeld, M.; Sgrott, O.L.; Taborda, M.A.; Koullapis, P.; Bauer, K.; Kassinos, S. Analysis of flow field and turbulence predictions in a lung model applying RANS and implications for particle deposition. *Eur. J. Pharm. Sci.* **2021**, *166*, 105959. [[CrossRef](#)] [[PubMed](#)]
97. Cimbala, J.M. *Fluid Mechanics*, 4th ed.; McGrawHill: New York, NY, USA, 2024.
98. Hubbe, M.A. Detachment of Colloidal Hydrous Oxide Spheres from Flat Solids Exposed to Flow 4. Effect of Polyelectrolytes. *Colloids Surf.* **1987**, *25*, 325–339. [[CrossRef](#)]
99. Blais, B.; Lassaigne, M.; Goniva, C.; Fradette, L.; Bertrand, F. Development of an unresolved CFD-DEM model for the flow of viscous suspensions and its application to solid-liquid mixing. *J. Comput. Phys.* **2016**, *318*, 201–221. [[CrossRef](#)]

100. Kravets, B.; Schulz, D.; Jasevicius, R.; Reinecke, S.R.; Rosemann, T.; Kruggel-Emden, H. Comparison of particle-resolved DNS (PR-DNS) and non-resolved DEM/CFD simulations of flow through homogenous ensembles of fixed spherical and non-spherical particles. *Adv. Powder Technol.* **2021**, *32*, 1170–1195. [[CrossRef](#)]
101. Qi, J.; Fei, W.B.; Narsilio, G.A. An LBM study on the local fluid flow in irregular monodisperse granular assemblies from DEM: Effects of particle shape. *Comput. Geotech.* **2025**, *177*, 106817. [[CrossRef](#)]
102. Wang, R.; Wu, F.; Fei, H.Q.; Wang, X.J.; Xu, H. Spectral proper orthogonal decomposition analysis of a spatially developing underexpanded round jet at $Re = 45\,000$. *Phys. Fluids* **2024**, *36*, 105195. [[CrossRef](#)]
103. Barea, G.; Jofre, L. Proper orthogonal decomposition of wall-bounded high-pressure transcritical fluids. *Phys. Fluids* **2024**, *36*, 105175. [[CrossRef](#)]
104. Mizuno, Y.; Komatsuzaki, T. Quantum algorithm for dynamic mode decomposition integrated with a quantum differential equation solver. *Phys. Rev. Res.* **2024**, *6*, 043031. [[CrossRef](#)]
105. Li, D.D.; Zhao, B.D.; Lu, S.; Wang, J.W. A data-driven method for fast predicting the long-term hydrodynamics of gas-solid flows: Optimized dynamic mode decomposition with control. *Phys. Fluids* **2024**, *36*, 103332. [[CrossRef](#)]
106. Xie, B.T.; Zhang, Q.; Lin, F.L.; Jin, W.F.; Cui, Z.J. Modal Decomposition of Internal Tides in the Luzon Strait through Two-Dimensional Fourier Bandpass Filtering. *J. Mar. Sci. Eng.* **2024**, *12*, 1477. [[CrossRef](#)]
107. Seifi, Z.; Raisee, M.; Cervantes, M.J. Global linear stability analysis of flow inside an axial swirl generator with a rotating vortex rope. *J. Hydraul. Res.* **2023**, *61*, 34–50. [[CrossRef](#)]
108. Mandal, D.; Lesur, M.; Gravier, E.; Sama, J.N.; Guillevic, A.; Sarazin, Y.; Garbet, X. Global linear stability analysis of kinetic trapped ion mode (TIM) in tokamak plasma using the spectral method. *Plasma Phys. Control. Fusion* **2023**, *65*, 055001. [[CrossRef](#)]
109. Mendis, R.L.A.; Sekimoto, A.; Okano, Y.; Minakuchi, H.; Dost, S. Global Linear Stability Analysis of Thermo-solutal Marangoni Convection in a Liquid Bridge Under Zero Gravity. *Microgravity Sci. Technol.* **2020**, *32*, 729–735. [[CrossRef](#)]
110. Heidt, L.; Colonius, T. Spectral proper orthogonal decomposition of harmonically forced turbulent flows. *J. Fluid Mech.* **2024**, *985*, A42. [[CrossRef](#)]
111. Hamzehloo, A.; Lusher, D.J.; Sandham, N.D. Direct numerical simulations and spectral proper orthogonal decomposition analysis of shocklet-containing turbulent channel counter-flows. *Int. J. Heat Fluid Flow* **2023**, *104*, 109229. [[CrossRef](#)]
112. Blanco, D.C.P.; Martini, E.; Sasaki, K.; Cavalieri, A.V.G. Improved convergence of the spectral proper orthogonal decomposition through time shifting. *J. Fluid Mech.* **2022**, *950*, A9. [[CrossRef](#)]
113. Rezaie, M.; Momen, M. Characterizing turbulence structures in convective and neutral atmospheric boundary layers via Koopman mode decomposition and unsupervised clustering. *Phys. Fluids* **2024**, *36*, 066605. [[CrossRef](#)]
114. Taga, K.; Kato, Y.; Yamazaki, Y.; Kawahara, Y.; Nakao, H. Dynamic mode decomposition for Koopman spectral analysis of elementary cellular automata. *Chaos* **2024**, *34*, 013125. [[CrossRef](#)] [[PubMed](#)]
115. Ilak, M.; Rowley, C.W. Modeling of transitional channel flow using balanced proper orthogonal decomposition. *Phys. Fluids* **2008**, *20*, 034103. [[CrossRef](#)]
116. Yu, D.; Chakravorty, S. A randomized balanced proper orthogonal decomposition technique. *J. Comput. Appl. Math.* **2020**, *368*, 112540. [[CrossRef](#)]
117. Chevalier, Q.; Douglas, C.M.; Lesshafft, L. Resolvent analysis of swirling turbulent jets. *Theor. Comput. Fluid Dyn.* **2024**, *38*, 641–663. [[CrossRef](#)]
118. Feng, D.C.; Gupta, V.; Li, L.K.B.; Wan, M.P. Resolvent analysis for predicting energetic structures in the far wake of a wind turbine. *Phys. Fluids* **2024**, *36*, 085101. [[CrossRef](#)]
119. Martini, E.; Schmidt, O. Stability and resolvent analysis of compressible viscous flows in MATLAB. *Theor. Comput. Fluid Dyn.* **2024**, *38*, 665–685. [[CrossRef](#)]
120. Rolandi, L.V.; Ribeiro, J.H.M.; Yeh, C.A.; Taira, K. An invitation to resolvent analysis. *Theor. Comput. Fluid Dyn.* **2024**, *38*, 603–639. [[CrossRef](#)]
121. Wan, K.D.; Huang, Y.Z.; Liu, R.T.; He, Y.; Lu, M.Q.; Jiang, C.W. Large eddy simulation of a swirling kerosene spray flame: A proper orthogonal decomposition and wavelet transform analysis on the flow structure and hydroxyl species field. *Phys. Fluids* **2024**, *36*, 093354. [[CrossRef](#)]
122. Yan, F.; Zhang, G.Q.; Rinoshika, A.; Song, B.; Zhang, J. A study on the wake structure of an ascending submersible with silk flexible appendages using continuous wavelet transform and dynamic mode decomposition. *Exp. Therm. Fluid Sci.* **2025**, *160*, 111323. [[CrossRef](#)]
123. Chang, C.W.; Lee, J.C.; Huang, W.C. Hydrological Data Projection Using Empirical Mode Decomposition: Applications in a Changing Climate. *Water* **2024**, *16*, 2669. [[CrossRef](#)]
124. Li, G.H.; Han, Y.Y.; Yang, H. A novel approach for underwater acoustic signal denoising based on improved time-variant filtered empirical mode decomposition and weighted fusion filtering. *Ocean Eng.* **2024**, *313*, 119550. [[CrossRef](#)]
125. Chen, H.S.; Liu, W.W.; Li, S.Q. A fully-resolved LBM-LES-DEM numerical scheme for adhesive and cohesive particle-laden turbulent flows in three dimensions. *Powder Technol.* **2024**, *440*, 119800. [[CrossRef](#)]

126. Zhou, Y.J.; Chen, L.P.; Gong, Y.F.; Wang, S.L. Pore-Scale Simulations of Particles Migration and Deposition in Porous Media Using LBM-DEM Coupling Method. *Processes* **2021**, *9*, 465. [[CrossRef](#)]
127. Putignano, C.; Burris, D.; Moore, A.; Dini, D. Cartilage rehydration: The sliding-induced hydrodynamic triggering mechanism. *Acta Biomater.* **2021**, *125*, 90–99. [[CrossRef](#)] [[PubMed](#)]
128. Biglarfadafan, M. Chapter 19—Artificial Intelligence including Machine Learning and Deep Learning algorithms. In *Advanced Tools for Studying Soil Erosion Processes*; Elsevier: Amsterdam, The Netherlands, 2024.

Disclaimer/Publisher’s Note: The statements, opinions and data contained in all publications are solely those of the individual author(s) and contributor(s) and not of MDPI and/or the editor(s). MDPI and/or the editor(s) disclaim responsibility for any injury to people or property resulting from any ideas, methods, instructions or products referred to in the content.